Improving the TanDEM-X Digital Elevation Model for flood modelling using flood extents from Synthetic Aperture Radar images

Article

Published Version

It is advisable to refer to the publisher's version if you intend to cite from the work.

CrossMark

Improving the TanDEM-X Digital Elevation Model for flood modelling using flood extents from Synthetic Aperture Radar images

David C. Mason [a,*], Mark Trigg [b], Javier Garcia-Pintado [c], Hannah L. Cloke [a,c], Jeffrey C. Neal [b], Paul D. Bates [b]

[a] Department of Geography and Environmental Science, University of Reading, Whiteknights, PO Box 227, Reading RG6 6AB, UK
[b] School of Geographical Sciences, University of Bristol, University Road, Bristol BS8 1SS, UK
[c] Department of Meteorology, University of Reading, Earley Gate, PO Box 243, Reading, RG6 6BB, UK

ABSTRACT

The topography of many floodplains in the developed world has now been surveyed with high resolution sensors such as airborne LiDAR (Light Detection and Ranging), giving accurate Digital Elevation Models (DEMs) that facilitate accurate flood inundation modelling. This is not always the case for remote rivers in developing countries. However, the accuracy of DEMs produced for modelling studies on such rivers should be enhanced in the near future by the high resolution TanDEM-X WorldDEM.

In a parallel development, increasing use is now being made of flood extents derived from high resolution Synthetic Aperture Radar (SAR) images for calibrating, validating and assimilating observations into flood inundation models in order to improve these. This paper discusses an additional use of SAR flood extents, namely to improve the accuracy of the TanDEM-X DEM in the floodplain covered by the flood extents, thereby permanently improving this DEM for future flood modelling and other studies.

The method is based on the fact that for larger rivers the water elevation generally changes only slowly along a reach, so that the boundary of the flood extent (the waterline) can be regarded locally as a quasi-contour. As a result, heights of adjacent pixels along a small section of waterline can be regarded as samples with a common population mean. The height of the central pixel in the section can be replaced with the average of these heights, leading to a more accurate estimate. While this will result in a reduction in the height errors along a waterline, the waterline is a linear feature in a two-dimensional space. However, improvements to the DEM heights between adjacent pairs of waterlines can also be made, because DEM heights enclosed by the higher waterline of a pair must be at least no higher than the corrected heights along the higher waterline, whereas DEM heights not enclosed by the lower waterline must in general be no lower than the corrected heights along the lower waterline. In addition, DEM heights between the higher and lower waterlines can also be assigned smaller errors because of the reduced errors on the corrected waterline heights.

The method was tested on a section of the TanDEM-X Intermediate DEM (IDEM) covering an 11 km reach of the Warwickshire Avon, England. Flood extents from four COSMO-SkyMed images were available at various stages of a flood in November 2012, and a LiDAR DEM was available for validation. In the area covered by the flood extents, the original IDEM heights had a mean difference from the corresponding LiDAR heights of 0.5 m with a standard deviation of 2.0 m, while the corrected heights had a mean difference of 0.3 m with standard deviation 1.2 m. These figures show that significant reductions in IDEM height bias and error can be made using the method, with the corrected error being only 60% of the original. Even if only a single SAR image obtained near the peak of the flood was used, the corrected error was only 66% of the original. The method should also be capable of improving the final TanDEM-X DEM and other DEMs, and may also be of use with data from the SWOT (Surface Water and Ocean Topography) satellite.

1. Introduction

Globally, flooding accounts for a substantial proportion of the fatalities and economic losses caused by natural hazards. Flood inundation models are commonly used to model river flooding, and are employed for damage assessment and flood defence design studies, flood relief

* Corresponding author.
  E-mail addresses: d.c.mason@reading.ac.uk (D.C. Mason), mark.trigg@bristol.ac.uk
(M. Trigg), j.garcia-pintado@reading.ac.uk (J. Garcia-Pintado), h.l.cloke@reading.ac.uk
(H.L. Cloke), j.neal@bristol.ac.uk (J.C. Neal), paul.bates@bristol.ac.uk (P.D. Bates).

management and improved flood forecasting. A basic requirement of a flood inundation model is a Digital Terrain Model (DTM) of the river reach being studied. Many floodplains in the developed world have now been imaged with high resolution airborne LiDAR or InSAR (Interferometric Synthetic Aperture Radar), giving accurate DTMs that facilitate accurate flood inundation modelling. For example, airborne LiDAR typically has a height accuracy of about 0.1 m at 1 m spatial resolution or better, sufficient for accurate flood modelling in urban areas (e.g. Neal et al., 2011). Such accuracy is generally not available in the case of remote rivers in developing countries. However, the accuracy of DTMs produced for modelling studies on such rivers should be enhanced in the near future by the availability of the high resolution TanDEM-X WorldDEM.

Yan, Di Baldassarre, Solomatine, and Schumann (2015) point out that there was a lack of globally-available DEM data for use as input data for hydraulic modelling before the launch of the Shuttle Radar Topography Mission (SRTM) in 2000. The SRTM DEM covers all land between 60N and 56S, about 80% of the Earth's land surface. Until recently the DEM pixel size has been 3 arc sec at the equator (about 90 m globally) and 1 arc sec (about 30 m) in the USA and Australia, though the latest release data are now 30 m globally. The relative height error ranges from 4.7 to 9.8 m at the continent scale (Rodríguez, Morris, & Belz, 2006). The SRTM heights include vegetation canopy heights so that the DEM is not a 'bare-earth' DTM. A number of studies have used the SRTM DEM for large-scale hydraulic modelling in river and delta areas (e.g. Sanders, 2007; Schumann et al., 2008; Alfieri et al., 2014; LeFavour, 2005; Neal, Schumann, & Bates, 2012; Patro, Chatterjee, Singh, & Raghuwanshi, 2009; Wang, Yang, & Yao, 2012; Yan, Di Baldassarre, & Solomatine, 2013). These have covered many aspects of hydraulic modelling, including water level and water surface slope retrieval, flood extent simulation and water level and discharge prediction. A further near-global DEM that could be used for flood modelling is that produced by the Advanced Spaceborne Thermal Emission and Reflection Radiometer (ASTER). This is a 30 m DEM produced by stereo-photogrammetry, whose second version (ASTER GDEM2) was released in 2011. However the vertical resolution of ASTER GDEM2 ranges from 7 to 14 m and the DEM contains anomalies and artefacts, leading to high elevation errors on local scales and so hampering its use for flood modelling purposes.

The new TanDEM-X DEM produced by DLR (German Aerospace Centre) will produce pole-to-pole coverage with unprecedented accuracy, and should eventually replace the SRTM DEM for large-scale hydraulic modelling. It will have a spatial resolution of 0.4 arc sec at the equator (10–12 m globally), and a relative height accuracy of less than 2 m on slopes less than 20% and 4 m on slopes greater than 40% (Eineder, Fritz, Jaber, Rossi, & Breit, 2012; Krieger et al., 2006). The global DEM is expected to be completed by the end of 2015 (Zink, 2012). Scientific assessment of the DEM is presently at an experimental stage, though there are already assessments of the Intermediate DEM (IDEM), the intermediate product of TanDEM-X based on only one coverage of the globe. Results show that, for the flat and sparsely vegetated terrain found in many floodplains, the IDEM accuracy achieved is better than the design specification (Gruber et al., 2012). As with SRTM, TanDEM-X measures heights to top of canopy, so is a Digital Surface Model (DSM) from which vegetation heights must be removed to create a DTM. First observations seem to indicate that the TanDEM-X DEM might allow for the first time more detailed local flood studies at the global scale (Yan et al., 2015). With the advent of very high resolution global flood modelling for risk management and forecasting, it is likely to be of great use in helping to improve predictions and decision making (e.g. Pappenberger, Dutra, Wetterhall, & Cloke, 2012; Bierkens et al., 2015; Beven, Cloke, Pappenberger, Lamb, & Hunter, 2015).

Fig. 1a shows the topography of a floodplain region in the UK mapped using airborne LiDAR at 2.5 m resolution. In contrast, Fig. 1b shows the SRTM tiles covering the same area at 90 m resolution, the

resolution that has been used by large-scale flood modelling studies using SRTM data to date. Fig. 1c shows the TanDEM-X IDEM tiles for the area, showing the great increase in resolution and accuracy provided by the TanDEM-X global DEM at 12.5 m resolution.

A further important data resource used in flood modelling is the extent of the flood and its variation over time. High resolution satellite SAR sensors are commonly used to acquire flood extents because they allow images to be taken from space over a wide area, can see through clouds, and can acquire images at night-time as well as during the day. Increasing use is now being made of SAR-derived flood extents for calibrating, validating and assimilating observations into flood inundation models in order to improve these (Mason, Garcia-Pintado, & Dance, 2014). Flood extents become more useful if they are intersected with the DTM of the floodplain (e.g. Raclot, 2006; Schumann, Neal, Mason, & Bates, 2011; Matgen et al., 2011; Garcia-Pintado, Neal, Mason, Dance, & Bates, 2013). Water level observations (WLOs) at the flood boundary can then be estimated at various points along a river reach, and these can be assimilated into a flood inundation model to keep the model 'on track' and improve the flood forecast. The floodplain DTM could be derived from the TanDEM-X DEM.
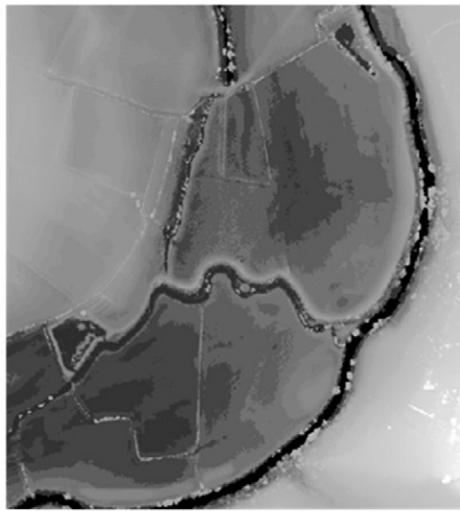
This paper discusses an additional use of SAR flood extents, namely to improve the height accuracy of the TanDEM-X DEM in the floodplain covered by the flood extents. This would permanently improve the DEM for future flood modelling and other studies of an area. A more accurate DEM would result in more accurate modelling and more accurate measurement of WLOs. Though in some cases (e.g. the use of a sub-grid model (e.g. Neal et al., 2012)), the TanDEM-X DEM might be spatially averaged to produce a DEM of lower resolution and higher accuracy, in others (e.g. modelling of urban flooding) the full resolution of the TanDEM-X DEM might be required. If it is required to extract WLOs from the SAR flood extents, these would be most accurate using the highest resolution of the TanDEM-X DEM.

The objective of the paper is to investigate the increase in height accuracy in the TanDEM-X IDEM that can be achieved in the floodplain area covered by the SAR flood extents using these extents.

2. Study area and data set

The method was tested on a section of the TanDEM-X IDEM covering an 11 km reach of the Warwickshire Avon, England (Fig. 2a). The TanDEM-X data used to construct the IDEM in this area were acquired when the river was in bank (based on readings from a local gauge), so that the floodplain was not flooded in the IDEM. Fig. 2b shows the height error map (1 standard deviation) associated with this section of IDEM, the errors being derived from interferometric coherence and geometrical considerations (DLR, 2011). No error reduction due to combination of different coverages is present for the IDEM. The error is considered to be a random error, but DLR (2011) cautions that there will be phase unwrapping errors that will only be resolved in the final DEM. The average slope of the river over this length was approximately 1×10^{-4}. Fig. 3 shows a land cover map of the area, which is largely rural with the town of Pershore just to the north of centre.

The test was based on an approximately 1-in-10-year flood event that occurred on the river in November 2012. Satellite SAR observations of the event were acquired by the COSMO-SKyMed (CSK) constellation (Garcia-Pintado et al., 2015). The 4-satellite polar orbiting C-band constellation was tasked by the authors. A sequence of 4 Stripmap images giving good synoptic views of the flooding was acquired on a daily basis covering the period 27–30 November 2012 (Fig. 4). The first image in the sequence was acquired just after the flood peak, and the subsequent images show the flood gradually receding. All CSK images were HH polarization, providing good discrimination between flooded and non-flooded regions. Details of the overpasses are given in Table 1.

(a)

(b)

0 10 20 30 40 50 m

(c)

Fig. 1. (a) LiDAR DEM of a sub-area of Fig. 2 (2.5 m pixels, 1 × 1 km), (b) SRTM DEM (90 m pixels), (c) TanDEM-X IDEM) (12.5 m pixels, © DLR 2007).
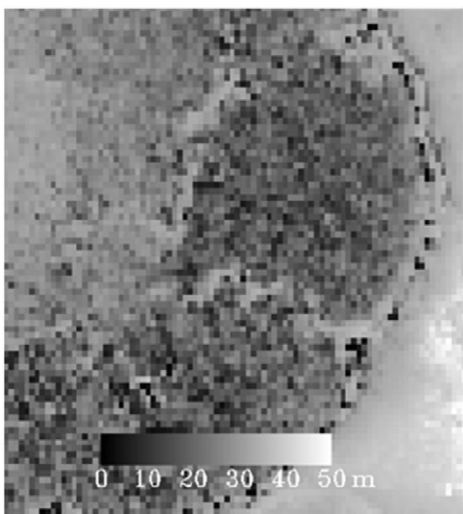
3. Method

3.1. Overview

The method used to increase the accuracy of the IDEM is based on the fact that for larger rivers the water elevation changes only slowly along a reach, so that the boundary of the flood extent (the waterline) can be regarded locally as a quasi-contour. As a result, heights of adjacent pixels along a small section of waterline can be regarded as a sample of heights with a common population mean. The height of the central pixel in the section can be replaced with the average of these heights, leading to a more accurate height estimate because a substantial portion of the IDEM height error is a random component.

While this will result in a reduction in the height errors along a waterline, the waterline is a linear feature in a two-dimensional space. However, improvements to the DEM heights between adjacent pairs of waterlines can also be made, because DEM heights enclosed by the higher waterline of a pair must be at least no higher than the corrected heights along the higher waterline (otherwise they would emerge from the flood extent), whereas DEM heights not enclosed by the lower waterline must be no lower (except in certain circumstances) than the corrected heights along the lower waterline. In addition, DEM heights between the higher and lower waterlines can also be assigned smaller errors because of the reduced errors on the corrected waterline heights. Note that no averaging of height values is performed in correcting heights between waterlines (so that no spatial resolution is lost), whereas the averaging of heights along waterlines is justified because the latter are locally isolines. The result is not the same as smoothing the height map using a square smoothing kernel in two dimensions, which would reduce spatial resolution.

The method consisted of five stages, as shown in Fig. 5:

(a) Pre-processing,
(b) Flood extent extraction,
(c) Candidate waterline pixel selection in rural areas,
(d) Correction of candidate waterline pixel heights,
(e) Adjustment of the IDEM between adjacent higher and lower waterlines.

3.2. Pre-processing

The 12.5 m resolution IDEM and its height error map were resampled to the 2.5 m resolution of the CSK images using nearest neighbour interpolation, so that blocks of 5 × 5 pixels in each downscaled map contained the same values (see Section 3.5).

The SAR images were processed to level 1C-GEC, which meant that they were geo-corrected to approximately100 m. It was necessary to register the images to British National Grid coordinates using ground control points and a digital map, when a registration accuracy of better than 2 pixels (of size 2.5 m) was obtained. The height error at a waterline pixel due to mis-registration should be small compared to the random error on an IDEM pixel height.

3.3. Flood extent extraction

It was important to minimize inaccuracies in the SAR flood extents extracted, as these might give rise to inaccuracies in the corrected IDEM.

In the absence of significant surface water turbulence due to wind, rain or currents, flood water generally appears dark in a SAR image because the water acts as a specular reflector, scattering radiation away from the satellite. This provides the basis of the flood detection approach. Detection of the flood extent in each image was performed
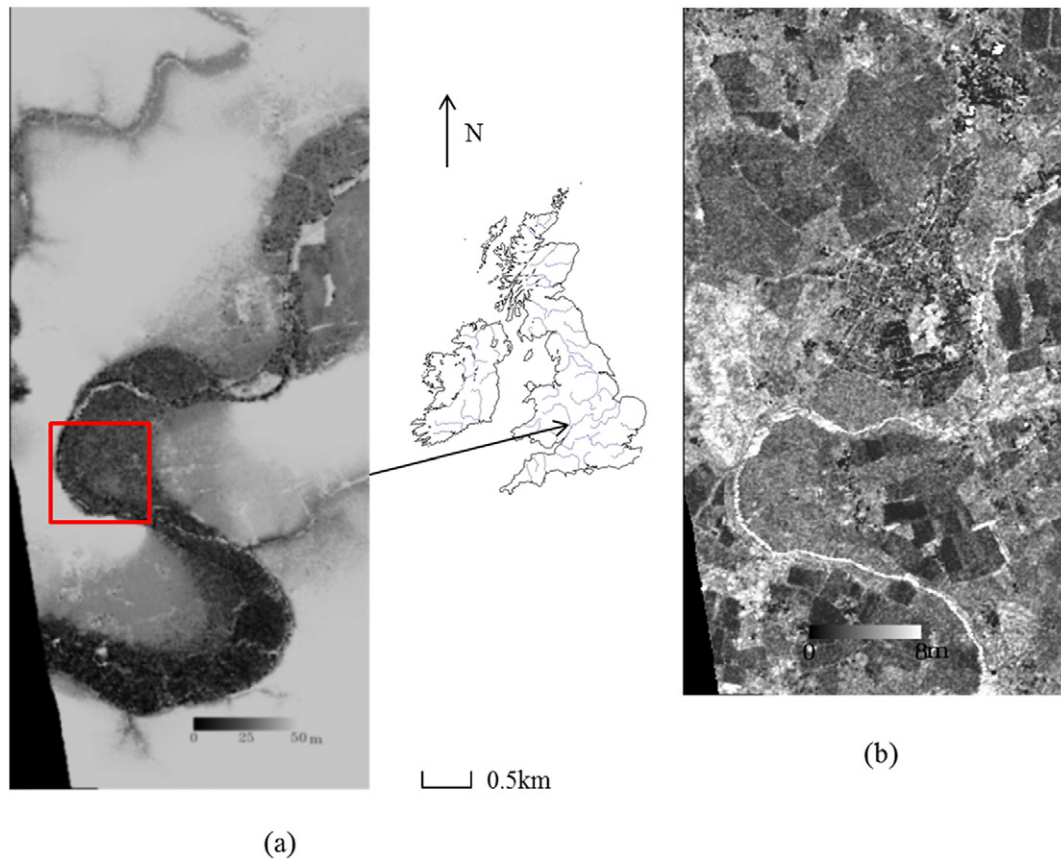
Fig. 2. (a) TanDEM-X IDEM of the flooded reach and, (b) IDEM height error map (1 standard deviation) of the flooded reach (lowest part not supplied) (© DLR 2014).

using the segmentation technique described in Mason, Davenport, Neal, Schumann, and Bates (2012a), which groups the very large numbers of pixels in the scene into homogeneous regions, and can cope with both rural and urban flood detection. As there was no flooding of urban areas in the flood event studied, only the rural flood detection algorithm was used. The scale parameters for the segmentation were the same as those used in Mason et al. (2012a), and also for segmentation of a number of SAR images of other floods around the world, from several different high resolution SAR sensors. A critical step is the automatic determination of a threshold on the region mean SAR backscatter, such that regions having mean backscatter below the threshold are classified as flooded, and others as un-flooded. The threshold determined was checked manually and corrected if necessary.

The initial rural flood classification was improved by refining it in a number of ways. For example, emergent vegetation adjacent to the flood such as hedgerows may produce a high rather than low SAR backscatter even though they are flooded. This is due to double scattering, whereby radar rays transmitted from the sensor to the water are reflected first to the hedgerow then back to the sensor (or vice versa). Accordingly, regions of high backscatter that were long, thin, fairly straight and adjacent to flood regions were automatically reclassified as flooded. It was verified that no urban areas (which might also have had high backscatter) were misclassified as flooded in this step. The backscatter threshold was also raised to include in the flood category regions of flooding adjacent to the flood class that had slightly higher mean backscatter than the original threshold (e.g., due to wind ruffling the water surface in more exposed parts of the floodplain). Note that no DTM information was used in the segmentation process.

Using contemporaneous aerial photographs, the algorithm has been shown to produce accurate flood inundation maps in rural areas, with about 90% of flooded pixels being classified correctly and only a few per cent of false positives (Mason et al., 2012a). This is similar to the

accuracies achieved by other researchers (e.g. Martinis, Twele, & Voigt, 2011).

Fig. 4 shows the flood extents detected in the images overlain on the SAR data in the IDEM sub-domain. While the flood extents appear largely correct, the fact that they are not perfect can be seen from the flooded fields misclassified as un-flooded in the north-east of the images near the river.

3.4. Candidate waterline pixel selection in rural areas

Candidate waterline pixels were selected from the flood extent in rural areas. As previously noted, sections of waterline in the interior of the flood extent caused by regions of emergent vegetation (e.g. hedges) may have erroneously low water levels associated with them. While most of these will have been removed at the segmentation stage, residual sections may still exist and must be removed prior to further processing. This was facilitated by performing a dilation and erosion operation on the binary flood extent, as described in (Mason, Schumann, Neal, Garcia-Pintado, & Bates, 2012b), whereby the extent was first dilated by 10 m, then eroded by the same amount. Waterline pixels were detected by applying a Sobel edge detector (Castleman, 1996) to the modified flood extent, and retaining only the external edge pixels. It was required that an edge pixel was present at the same location before and after dilation and erosion, in order to select for true waterline segments on straighter sections of exterior boundaries in the flood extent.

To cope with the fact that in some regions there were systematic as well as random errors in the IDEM, false positives were also suppressed by several further methods. Firstly, a slope map was derived from the DEM and waterline points were only selected in regions of low or medium DEM slope. A waterline point may be heighted more accurately if it lies on a low slope rather than a high slope because a given error in its
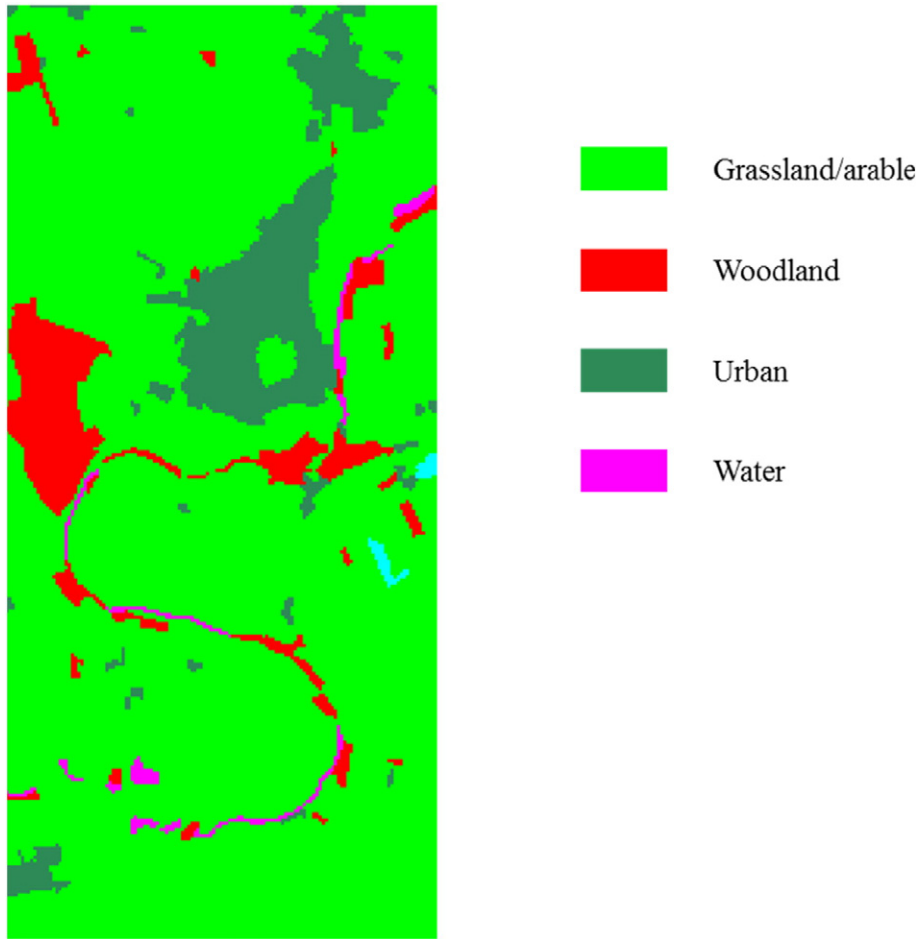
Fig. 3. Land cover map for the IDEM domain.

position will cause only a small error in height. The slope threshold was set quite high (0.6) because there was substantial noise in the IDEM slope values due to the large random error in the IDEM heights (see below).

Secondly, allowance was made for the fact that the IDEM is a DSM rather than a 'bare-earth' DTM. Ideally the IDEM should be processed to remove the heights of surface objects to leave a DTM that can be used in the subsequent processing. This step was approximated in this case by using the land cover map to select only candidate waterline pixels in regions of short vegetation, namely grassland and arable classes (Fig. 3). This map was a sub-section of the CEH Land Cover Map, constructed from high resolution multispectral satellite data (Morton et al., 2011). The original map containing 25 m pixels was downscaled to produce 2.5 m pixels to correspond to the CSK pixel size. The majority of the floodplain in the study area was comprised of grassland or arable classes. Note that the flood extent was measured to the position at which the short vegetation just emerged from the floodwater, so that if the vegetation height varied along the waterline, the assumption that the waterline heights were locally the same might have been violated (Horritt, Mason, Cobby, Davenport, & Bates, 2003). To overcome this problem, a method that used double scattering to correct rural waterline positions and levels due to the presence of emergent vegetation at the flood edge was employed in (Mason et al., 2012b). However, this was felt to be too elaborate for the current study given the likely short vegetation heights, and it was assumed that any height error due to the failure to remove short vegetation heights would be small compared to the IDEM random height error.

Finally, candidate water line pixels were required to lie within a certain height range centred on the mean water height in the area. In order to find the allowed waterline level range in the area, a histogram was constructed of the waterline levels, and the position of the mean was found. A normal distribution $N(\mu, \sigma^2)$ was fitted around the mean μ, and candidate waterline points with levels more than 2.5σ away from μ were suppressed.

3.5. Correction of candidate waterline pixel heights

For each candidate waterline pixel, a sample of adjacent heights was selected from an $n \times n$-pixel window in the 12.5 m IDEM space centred on the candidate. However, the processing at this stage was in the 2.5 m CSK image space, so only one pixel height in each 12.5 m IDEM pixel was selected to avoid introducing spurious height correlations. The use of nearest neighbour interpolation in the pre-processing stage (Section 3.2) ensured that, within each 12.5 m IDEM pixel, all 2.5 m CSK image space pixels had the height of the IDEM pixel. Provided sufficient adjacent heights were detected, their mean and standard deviation were estimated. If the standard deviation was less than that of the central pixel in the IDEM height error map, the central pixel's height was corrected to be the mean of the adjacent heights, and its IDEM height error map entry was updated. This seemed a reasonable approach given that the corrected mean height and height standard deviation estimates should be robust because they have been constructed from a set of samples. If a corresponding LiDAR height existed at this location, this was noted for validation purposes. It would be interesting to compare the results of this approach with those of a more complicated data-driven smoothing algorithm capable of choosing an optimal window size (e.g. Kervrann, 2004).

2012-11-27

2012-11-28

2012-11-29

2012-11-30

Fig. 4. Flood extents (blue) for the event of November 2012 overlain on SAR imagery of the flooded 11 km reach (© CSK).

A value for n of 11 in the 12.5 m IDEM space was chosen by experiment. This ensured that adjacent heights were sufficiently local that they were likely to form an isoline section, but also that close to the maximum possible number of candidate pixel heights were corrected. Values of n less than 11 tended to produced higher height standard deviations and correct fewer pixels (because a minimum of 4 adjacent heights was required), whereas values greater than 11 produced little reduction in standard deviation compared to that for $n = 11$. The latter is likely to be because the waterline is only a quasi-contour because there is a fall in water elevation moving downstream along the river, and this fall may not be linear over a long distance. The average number of adjacent heights employed was 11.

3.6. Adjustment of the IDEM between adjacent higher and lower waterlines

Each pair of adjacent waterlines in the time sequence was examined to update the section of IDEM between the current pair of waterlines if possible. No averaging of height was performed in correcting heights between waterlines, so that spatial resolution was maintained. The updating process was based on the heights and height errors associated with the candidate waterline pixels on the waterline pair. All IDEM pixels between the waterlines in the grassland or arable classes were first modified using the higher waterline of the pair wherever possible. If an IDEM pixel (of height h_i and error σ_i) had a height that exceeded that of the nearest candidate waterline pixel on the higher waterline, the IDEM pixel height ($h_i{}'$) and error ($\sigma_i{}'$) were set to those of the waterline pixel (h_w, σ_w).

$$h_i{}' = h_w \tag{1}$$

$$\sigma_i{}' = \sigma_w. \tag{2}$$

A distance-with-attribute transform was used to find the nearest candidate waterline pixel and its height. The distance-with-attribute transform is a form of distance transform that stores for each pixel in the transform image its distance to the nearest waterline point, and also the attribute (height) at that pixel (Mason, Scott, & Wang, 2006). The transform considered candidate waterline pixels from both banks of the river in selecting the nearest waterline pixel. If the IDEM pixel height (h_i) was less than that of the nearest waterline pixel, its height was not modified, but its height error could be reduced to $\sigma_i{}'$ if the upper bound (2 standard deviation level) of the IDEM pixel height was greater than that of the waterline pixel height i.e. if

$$h_i + 2\sigma_i > h_w + 2\sigma_w \tag{3}$$

using

$$\sigma_i{}' = |\, h_w + 2\sigma_w - h_i \,|/2 \tag{4}$$

where $\sigma_i{}'$ is obtained by equating the two sides of Eq. (3). In either case, the nearest candidate waterline pixel was required to lie within 250 m of the IDEM pixel for updating to occur. Again, corresponding LiDAR heights were noted for validation purposes.

The IDEM pixels between the waterlines were then modified if possible using the lower waterline of the pair, using similar rules to the above (though see below), in conjunction with the candidate waterline pixel heights and errors of the lower waterline. If an IDEM pixel in the grassland or arable classes had a height that was lower than that of the nearest candidate waterline pixel on the lower waterline, the IDEM pixel height ($h_i{}'$) and error ($\sigma_i{}'$) were set to those of the waterline pixel (h_w, σ_w). If not, its height was not modified, but its height error could be reduced to $\sigma_i{}'$ if

$$h_i - 2\sigma_i < h_w - 2\sigma_w \tag{5}$$

Table 1
Details of COSMO-SkyMed overpasses.

Time (UTC)	Pass	Incidence angle
27/11/12 19:20	Descending	49°
28/11/12 18:01	Descending	51°
29/11/12 18:20	Descending	32°
30/11/12 19:32	Descending	53°

using

$$\sigma_i{}' = |\, h_w - 2\sigma_w - h_i \,|/2 \tag{6}$$

where $\sigma_i{}'$ is obtained by equating the two sides of Eq. (5).

However, a complication arises because the situation for IDEM pixels below the lower waterline is not the same as that for pixels above the higher waterline. In the latter case, pixels must be at least no higher than the corrected heights along the higher waterline, otherwise they would emerge from the flood extent. The method for the lower waterline assumes that there is a monotonic increase in height between the lower and higher waterlines. Another possible scenario is that, moving away from the lower waterline, there is initially a rise in height that is followed by a fall to below the lower waterline, before the IDEM rises again to the height of the higher waterline. An extreme example might be if the lower waterline was obtained when the river was in bank, and a river embankment was protecting lower ground on the floodplain. In this case, no candidate waterline pixels would be selected from the lower waterline because they would lie on too high a slope. However, a less extreme rise followed by a fall is certainly possible. To cope with this, if an IDEM pixel height was below the level of the lower waterline, its neighbours were examined to see if they were significantly lower than this level also, and the IDEM pixel height was only raised to the lower waterline level if they were not. The average height and standard deviation of the 8 neighbours of the IDEM pixel were calculated, and this height and standard deviation were compared to the height and standard deviation of the local lower waterline using Welch's t-test (i.e. assuming unequal variances) to test whether the average height of the neighbours was significantly lower than that of the local waterline.

An important requirement of the method was that locally the higher waterline of the pair should never be lower than the lower waterline, and to this end lower waterline candidate pixels higher than nearby higher waterline candidate pixels were suppressed in a pre-processing step.

In addition, any IDEM pixels enclosed within the lowest waterline boundary were assessed for possible modification so that locally they did not exceed this waterline height. On the other hand, no attempt was made to modify IDEM pixels outside the boundary of the highest waterline that were lower than the highest waterline. This was because, for example, an embankment might have been present at the edge of the highest flood extent, so that, even if lower areas of floodplain were present beyond the embankment, these would not be covered by water.

In the above method, pixel heights between the waterlines were only modified if they lay above the higher or below the lower waterline of a pair. One consequence of this was that the upper and lower height errors associated with a height could be different. An alternative method that was also studied involved modifying the height to lie at the centre of its associated error range, so that the upper and lower height errors once again became the same.

4. Results

On average about 45% of the waterline pixels in each flood extent became candidate pixels able to satisfy the selection criteria of having a low/medium slope, not being a height outlier, and coinciding with short vegetation.
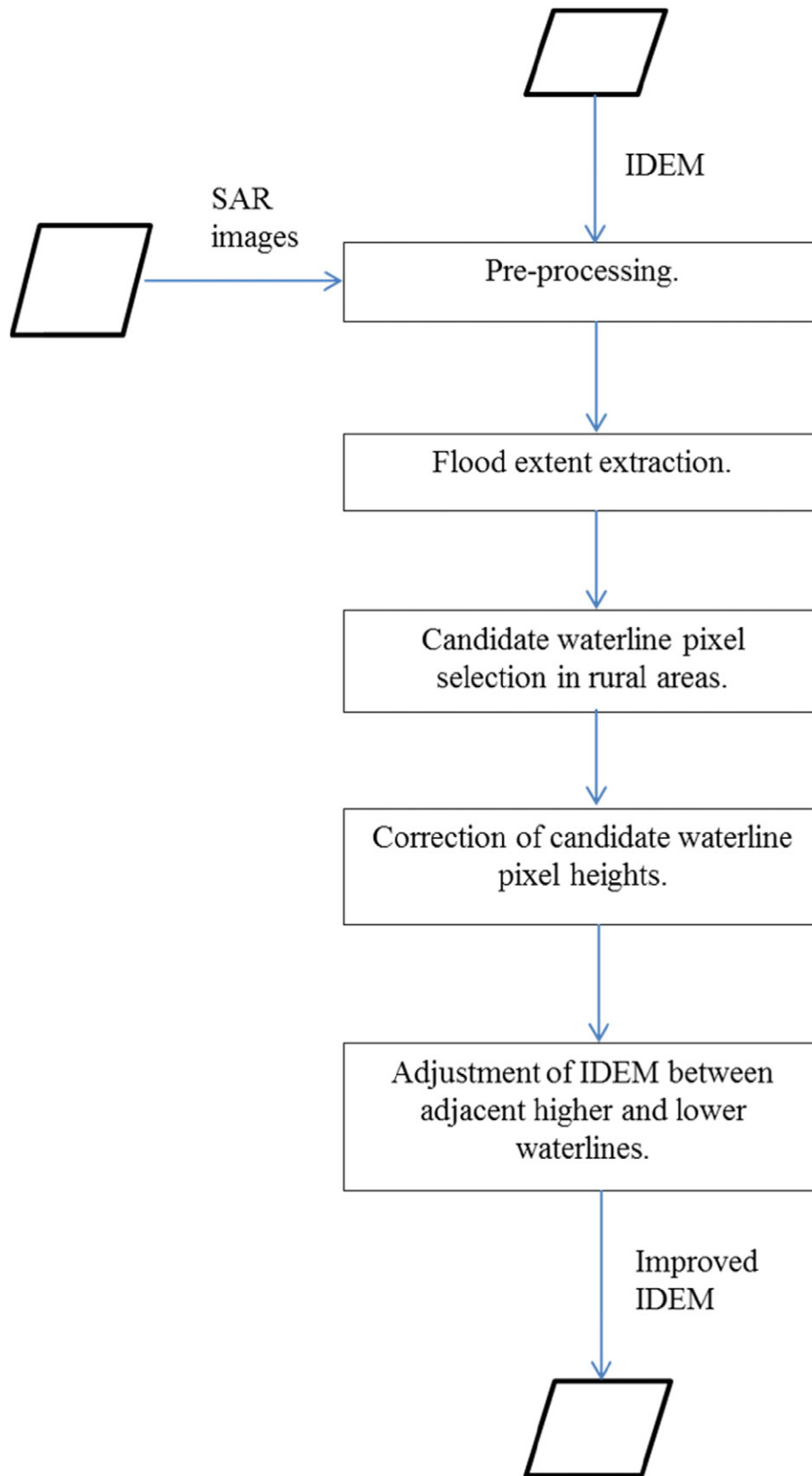
Fig. 5. Steps in the processing chain.

Original and corrected IDEM candidate waterline pixel heights were compared to corresponding airborne LiDAR heights (Table 2). The mean waterline height fell by about 0.5 m between successive waterlines as the flood receded. Averaged over the four waterlines considered, it was found that the difference between the original IDEM candidate pixel heights and the corresponding LiDAR heights had a standard deviation of 1.25 m and a bias (i.e. a difference from zero) of 0.38 m, while for the corrected heights the difference had a standard deviation of

Table 2
Comparison of original and corrected IDEM waterline heights to LiDAR validation heights.

Image date	Mean waterline height (m)	No. of pixels validated	Mean difference of original height from LiDAR height (m)	Standard deviation of difference of original height from LiDAR height (m)	Mean difference of corrected height from LiDAR height (m)	Standard deviation of difference of corrected height from LiDAR height (m)
20121127	15.27	3934	0.38	1.17	0.36	0.73
20121128	14.76	3567	0.43	1.32	0.43	0.82
20121129	14.16	3255	0.39	1.20	0.37	0.69
20121130	13.58	1742	0.30	1.29	0.33	0.71

only 0.74 m and a similar bias. The corrected heights therefore have a standard deviation only 59% that of the original heights.

A floodplain area of 4.3 km^2 was covered by the waterlines along the 11 km reach. Considering the IDEM pixels between the waterlines in the grassland or arable classes that were modified, 33% of IDEM heights were above the higher waterline, and 30% below the lower waterline of an adjacent pair (Table 3). About 450,000 LiDAR heights were available in this area to validate the corresponding IDEM heights. When compared to LiDAR, the original heights that were above the higher waterline had a mean difference from the corresponding LiDAR heights of 1.60 m with standard deviation 2.10 m, while after correction the mean difference was 0.19 m with standard deviation 0.86 m. The corrected heights below the lower waterline were similarly improved, with the original heights having a mean difference from the LiDAR of −0.58 m with standard deviation 1.00 m, and the corrected having a mean difference of 0.28 m with standard deviation 0.61 m. About 8% of pixels were not modified below the lower waterline because their neighbours were significantly lower than the lower waterline. Considering the 63% of pixels whose heights were modified in this way, the original heights had a mean difference from the LiDAR of 0.61 m with standard deviation 2.05 m, while after correction the mean difference was 0.26 m with standard deviation 0.74 m. The height errors of a further 23% of IDEM heights between the higher and lower waterlines were also reduced, because of the reduced errors on the corrected waterline heights. The mean error of the original heights was 1.13 m, whereas the mean error of the corrected heights was 0.79 m (Table 4).

The overall improvement in accuracy of all the IDEM heights covered by the flood extents in the grassland or arable classes was also calculated. The original IDEM heights had a mean difference from the corresponding LiDAR heights of 0.48 m with a standard deviation of 1.97 m. The corrected IDEM heights had a mean difference from the LiDAR of 0.25 m with standard deviation 1.19 m. These figures show that significant reductions in IDEM height bias and error can be made using the local corrections involved in the method, with the corrected error being only 60% of the original. A caveat here is that the SAR waterline heights used to correct the IDEM are measured to the top of vegetation (see Section 3.4) while the LiDAR may be measuring heights closer to the ground surface. However, large areas of the floodplain in the study area are covered with short grass used for grazing, and the fact that this is present rather than there being a 'bare-earth' DTM should have little effect on this result.

Fig. 6a shows the original IDEM of the red square in Fig. 2a, and Fig. 6b shows the corrected IDEM for this area. In the area covered by

the waterlines, the corrected IDEM is smoother than the original. Its blocky nature in the corrected areas is due to the form of modification employed in the correction, with heights being rounded down/up to a higher/lower waterline. At the same time, the standard deviation and bias of the corrected heights are significantly reduced compared to their original counterparts. This is because the tails of the distribution of the differences of the corrected IDEM heights from the LiDAR heights have been truncated in the rounding process. Fig. 6c shows the original height error map. The method may produce asymmetric corrected height errors, and Fig. 6d shows the upper height error map (i.e. the error above the height estimate at a pixel), and Fig. 6e the lower height error map. The corrected errors in the area covered by the waterlines are generally substantially lower than the original errors.

The results for the alternative method of height correction in which a corrected IDEM height was modified to lie at the centre of its associated error range, so that its upper and lower height errors were symmetric, are given in Table 5. For the 63% of pixels between the waterlines in the grassland/arable class whose heights were modified, the symmetric error method gave height differences from the LiDAR of mean 0.25 m and standard deviation 1.05 m, while the corresponding figures for the asymmetric error method were 0.26 m and 0.74 m. For the 23% of pixels between the waterlines whose heights were not modified but reduced in error, the mean and standard deviation for the symmetric error method were 0.05 m and 1.31 m, while those for the asymmetric method were 0.17 m and 0.95 m. Therefore the asymmetric error method produces a reduced error compared to the symmetric error method, though this advantage is tempered by the fact that the method gives different upper and lower height errors.

A difficulty in the implementation of the method is the need to acquire a sequence of SAR images over the period of the flood. The 4 images used here are part of a larger sequence of 7 scenes imaging the flood over the wider Severn-Avon river network. While this is possibly the best example of the sequential monitoring of flood extent by high resolution SAR currently available, its acquisition involved considerable effort. Therefore the effect of reducing the number of images used to correct the IDEM was also studied. Instead of there being 4 SAR images each separated by 1 day, it was assumed that only 2 SAR images were available, on 27/11/2012 and 30/11/2012, so that the separation was 3 days and the mean waterline height difference between the 2 flood extents was 1.69 m (Table 2). This time separation is similar to the revisit interval specified for the 2-satellite Sentinel-1 constellation at the equator (in interferometric wide-swath mode assuming that ascending and descending passes and overlaps are used). Table 6 shows that, if
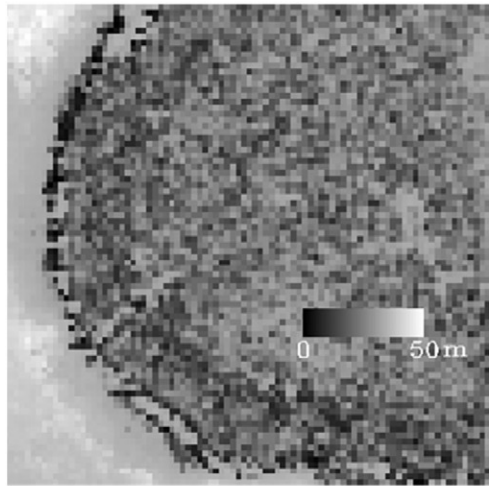
Table 3
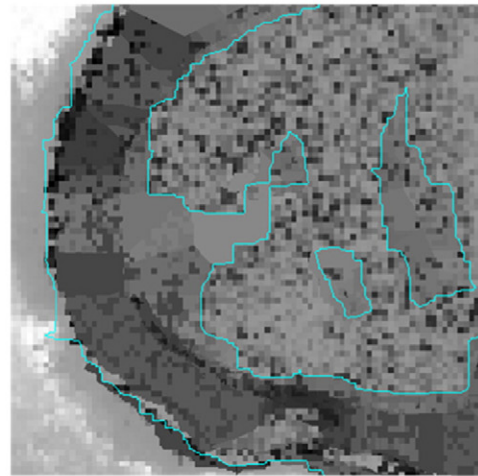Correction of modified IDEM pixel heights and errors between the waterlines.

Class	Percentage (%)	Mean difference of original IDEM heights and LiDAR heights (m)	Standard deviation of difference of original heights and LiDAR heights (m)	Mean difference of corrected IDEM heights and LiDAR heights (m)	Standard deviation of difference of corrected heights and LiDAR heights (m)
Pixel heights modified above an upper waterline	33	1.60	2.10	0.19	0.86
Pixel heights modified below a lower waterline	30	−0.58	1.00	0.28	0.61
Total pixel heights modified	63	0.61	2.05	0.26	0.74

Table 4
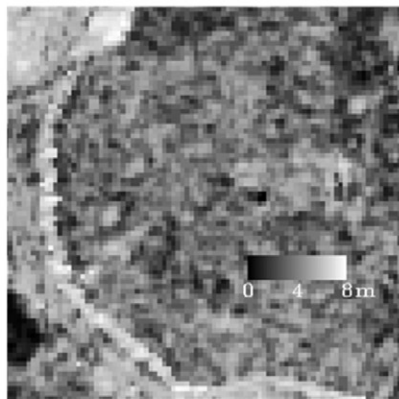Errors for IDEM pixel heights between the waterlines not modified but reduced in error.

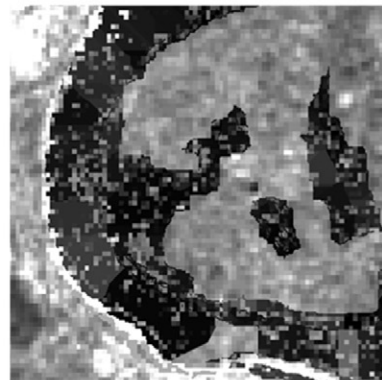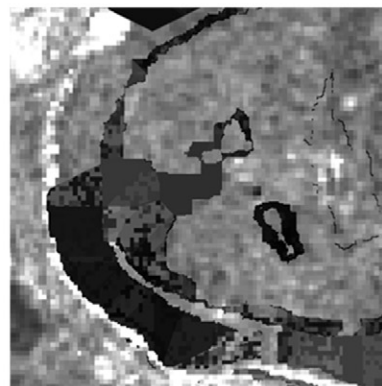| Class	Percentage (%)	Mean standard deviation of original heights (m)	Mean standard deviation of corrected heights (m)
Pixel heights not modified but reduced in error	23	1.13	0.79

Fig. 6. (a) Original IDEM of the red square in Fig. 2a (© DLR 2014), (b) IDEM corrected using sequence of four SAR images (the blue line is the highest SAR waterline, demarcating the corrected area), (c) original height error map, (d) corrected upper error map, and (e) corrected lower error map.

Table 5
Comparison of results using asymmetric and symmetric errors.

Class	Percentage (%)	Mean difference of original IDEM heights from LiDAR heights (m)	Standard deviation of difference of original heights from LiDAR heights (m)	Asymmetric errors		Symmetric errors	
				Mean difference of corrected IDEM heights from LiDAR heights (m)	Standard deviation of difference of corrected heights from LiDAR heights (m)	Mean difference of corrected IDEM heights from LiDAR heights (m)	Standard deviation of difference of corrected heights from LiDAR heights (m)
Pixel heights modified	63	0.61	2.05	0.26	0.74	0.25	1.05
Pixel heights not modified but reduced in error	23	0.17	0.98	0.17	0.98	0.05	1.31

IDEM heights both above the higher and below the lower waterline are modified, the standard deviation of the difference between the corrected IDEM heights and the corresponding LiDAR heights was 65% that of the original IDEM heights. While this represents a reduction in accuracy compared to the 60% achieved using 4 SAR images, it shows that a significant increase in IDEM height accuracy can still be achieved using 2 SAR images. Table 6 also shows, for the case of 2 images, the effect of not correcting heights lying below the lower waterline, and indicates that the result was improved if the correction was applied.

Simplest of all to acquire would be a single SAR image obtained near the peak of the flood. In this case IDEM heights within the flood extent could only be corrected above the waterline. A surprising result was how much correction could be achieved using only the single SAR image of 27/11/2012. Table 6 shows that, for this case, the standard deviation of the difference between the corrected IDEM heights and the corresponding LiDAR heights was 66% that of the original IDEM heights. This is only slightly worse than for the 2-image case, though the latter is able to modify heights below the lower waterline for IDEM pixels lying between the higher and lower waterlines, and also should be able to modify more accurately IDEM heights above the lower waterline and contained within it. It appears that using two images rather than one has in this case introduced more errors that have tended to offset the increased accuracy that should be obtainable. Fig. 7 shows, for the red square of Fig. 2a, the corrected IDEM using the single SAR image, together with the upper and lower height error maps, and compares these to the original IDEM height and error maps. Note that only the corrected upper height errors are reduced in the area covered by the flood extent (Fig. 7d); the corrected lower height errors (Fig. 7e) are not reduced because no modification can be applied to heights below the waterline in this case.

5. Discussion and conclusions

It is important to point out that the method is likely to work best on the relatively smooth topography found in many lowland river systems. Errors can arise in the height corrections for a number of reasons, including errors in the flood extents, in the candidate waterline pixel heights, and in the adjustment of IDEM heights and errors between adjacent waterlines. For example, in rough terrain with slopes greater than the slope threshold (0.6 (31°)), no candidate waterline pixels on low slopes would be found, and no corrections to the IDEM would be made. Again, in terrain with more undulating slopes of less than 31°,

the dilation/erosion operation carried out on the binary flood extent in stage (c) would incorrectly filter out small ridges rising above the local terrain and less than 20 m wide, and the heights of these would be incorrectly modified to the adjacent waterline height. Future work should aim in particular at developing an improved method of delineating the flood extent in the SAR image. Nevertheless, despite these limitations, the results show that, in the type of terrain encountered in the test area, the method is capable of making significant reductions in height bias and error in the Intermediate TanDEM-X IDEM in the area covered by the SAR flood extents. For the sequence of 4 SAR images, the corrected IDEM height error was only 60% that of the original. Even if the method employed only a single SAR image, the corrected IDEM height error was still only 66% of the original.

The method should also be able to improve the final TanDEM-X DEM when this becomes available. The height accuracy in the final DEM will undoubtedly be an improvement over that of the IDEM, in both low slope floodplain areas and on higher slopes, because the IDEM does not have the advantages of dual- (or multi-baseline) techniques or multiple incidence angles. A consequence of this in mountainous areas is that phase unwrapping errors may be present. These should be reduced in the final TanDEM-X DEM (DLR, 2011; Gruber et al., 2012).

A further interesting question is how the results change when the spatial resolution of the IDEM is coarsened. Over large floodplains, a modeller might want to reduce the resolution of the DTM to reduce height noise and enable faster modelling. To answer this, ideally the method should be tested on the final 0.4 arc sec (≈12 m) TanDEM-X DEM, and the final 1 arc sec (≈30 m) TanDEM-X DEM, together with their associated error maps, and the results compared. These are not yet available, and simply performing an averaging of the IDEM and combining adjacent errors in the IDEM height error map would not give values representative of the final 30 m DEM. Some qualitative insight into what might happen has been obtained by averaging the IDEM and combining adjacent errors in the IDEM height error map using a 3×3-pixel window. It was found that the standard deviations of the differences of the averaged original heights from the corresponding LiDAR heights reduced from those given in Table 2 as expected, due to the smoothing. Smoothing also caused a small increase in the means of the differences of the averaged original heights from the LiDAR heights compared to those of Table 2. However, the standard deviations of the differences of the corrected heights from the LiDAR heights were still reduced compared to those for the original heights, though not by as much as in Table 2, so that the method is still likely to produce an

Table 6
Comparison of results using different combinations of SAR images.

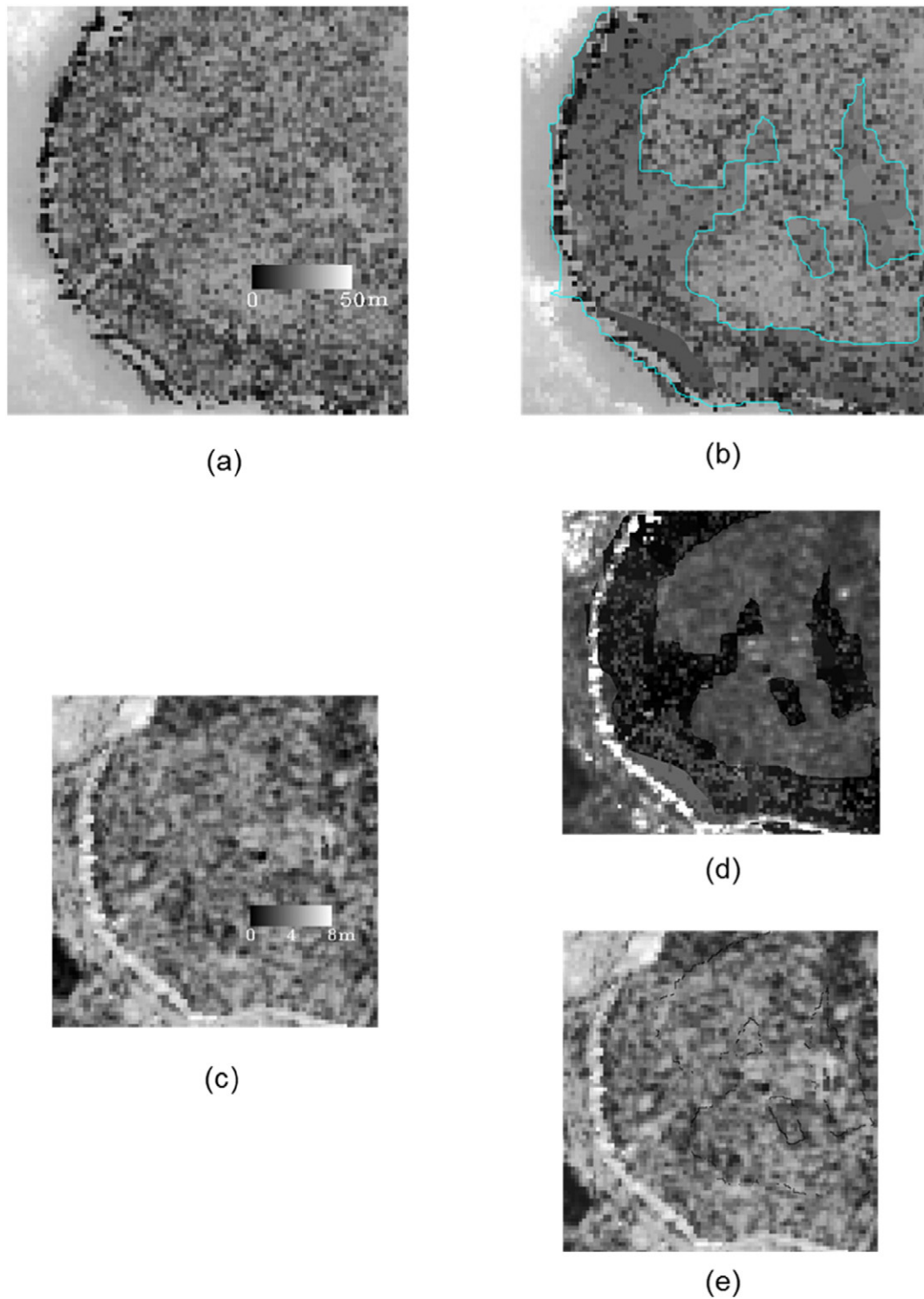| Number of SAR images	Dates in 11/2012	Correction of heights below lower waterline?	Mean difference of original IDEM heights from LiDAR heights (m)	Standard deviation of difference of original heights from LiDAR heights (m)	Mean difference of corrected IDEM heights from LiDAR heights (m)	Standard deviation of difference of corrected heights from LiDAR heights (m)	Percentage of corrected standard deviation to original standard deviation (%)
4	27, 28, 29, 30	Yes	0.48	1.97	0.25	1.19	60
2	27, 30	Yes	0.46	1.95	0.16	1.26	65
2	27, 30	No	0.46	1.95	0.03	1.34	73
1	27	Not applicable	0.45	1.93	0.01	1.27	66

Fig. 7. (a) Original IDEM of the red square in Fig. 2a (© DLR 2014), (b) IDEM corrected using single SAR image of 27/11/2012 (the blue line is the SAR waterline, demarcating the corrected area), (c) original height error map, (d) corrected upper error map, and (e) corrected lower error map.

improvement in the DEM. Further work should examine the effect on the method of coarsening the DEM resolution using the final DEMs in a more rigorous fashion.

Obviously a variety of algorithms could be used to estimate the heights of IDEM pixels between the waterlines, not just the asymmetric and symmetric error methods investigated above. The asymmetric error method involved the rounding of heights between waterlines up or

down to the relevant waterline to maintain spatial resolution, though methods involving smoothing followed if necessary by rounding could also be considered.

A caveat regarding the method is its effect on dykes adjacent to the river, which the water elevation in the river must exceed in order for water to spill onto the floodplain. A dyke might be too narrow to be visible in the IDEM given its 12.5 m pixel size, even though it might be

visible in the SAR image. However, if the dyke width was substantial compared to the IDEM pixel, the dyke could be inadvertently removed from the flood extent in the dilation/erosion operation carried out in stage (c). If the mean dyke height exceeded that of the lowest waterline (which might occur on a receding flood), some dyke heights could be incorrectly rounded down to the waterline height. To prevent this occurring, the river width could be masked out when performing the correction procedure. A global-scale width database for large rivers is currently being developed (Yamazaki et al., 2014).

Although the method presented here has been aimed at improving the TanDEM-X DEM in a river floodplain, it could also be used to improve the DEM in an inter-tidal zone, using a sequence of high resolution SAR images obtained at varying states of the tide between the high and low water marks (e.g. Mason et al., 1999; Thornhill, Mason, Dance, Lawless, & Nichols, 2012).

It could be applied to a variety of DEMs used for flood inundation modelling other than the TanDEM-X DEM, employing flood extents from higher resolution images at both microwave and optical wavelengths from a variety of satellite and aerial platforms (e.g. SRTM DEM data could be corrected using Sentinel-1 SAR flood extents).

The method should also have relevance for the SWOT (Surface Water and Ocean Topography) satellite to be launched in 2020 (JPL, 2015a; JPL, 2015b). SWOT will provide global coverage of floods every 11 days, with many locations sampled several times during this period. During its projected 3.5-year lifetime, it will generate an enormous amount of data on global flooding. It will generate a global water mask at each pass with a pixel size between 10×60 m and 10×10 m depending on position in swath, and this will contain rivers of width greater than 50 m. This mask image could be used to improve the TanDEM-X DEM (or at least its lower-resolution versions) in the same way as any other high resolution SAR image. Also, a goal of the mission is to produce a global DEM of all land elevations constructed from many SWOT orbits. The height accuracy of this DEM cannot yet be specified, though ideally it will be better than 1 m. A further requirement is that river height accuracy shall be 0.1 m or better over an area of 1 km^2 inside the water mask, using height averaging over this area. In addition, therefore, it might be possible to apply the method presented here to improve the SWOT DEM in flood-plain areas using SWOT water masks to generate heighted waterlines. The height averaging along waterlines used for TanDEM-X would effectively have been carried out in the height averaging over the water mask, but the method would still be useful in the subsequent DEM modification process between pairs of adjacent waterlines.

Future work should involve investigating the improvement in accuracy obtainable in the final TanDEM-X WorldDEM and its lower-resolution versions. The use of the corrected DEM in a flood inundation modelling study on a remote river system should also be investigated to determine the benefit of the method for modelling. There are many sources of error in this type of modelling other than DEM errors, including errors in input flow rates, channel and floodplain friction coefficients, river bathymetry and scale-dependent errors. Effort would be concentrated on high resolution modelling and accurate water level observation. The objective of this study would be to measure the impact of the reduced DEM errors in the context of the other errors.

Acknowledgements

References

Alfieri, L., Salamon, P., Bianchi, A., Neal, J., Bates, P., & Feyen, L. (2014). Advances in pan-European flood hazard mapping. *Hydrological Processes*, 28(13), 4067–4077. http://dx.doi.org/10.1002/hyp.9947.

Beven, K., Cloke, H., Pappenberger, F., Lamb, R., & Hunter, N. (2015). Hyperresolution information and hyperresolution ignorance in modelling the hydrology of the land surface. *Science China Earth Sciences*, 58(1), 25–35.

Bierkens, M. F. P., Bell, V. A., Burek, P., Chaney, N., Condon, L., David, C. H., ... Wood, E. F. (2015). Hyper-resolution global hydrological modelling: What is next? *Hydrological Processes*, 29, 310–320. http://dx.doi.org/10.1002/hyp.10391.

Castleman, K. R. (1996). *Digital image processing.* New Jersey: Prentice Hall.

DLR (2011). TanDEM-X DEM products specification document. Available at: https://tandemx-science.dlr.de/.../TD-GS-PS-0021_DEM-Product-Specification_v3.0.pdf.

Eineder, M., Fritz, T., Jaber, W., Rossi, C. & Breit, H. (2012). Decadal earth topography dynamics measured with TanDEM-X and SRTM. Proc. IGARSS Symp., Munich, Germany, July 22–27, 2012.

Garcia-Pintado, J., Mason, D. C., Dance, S. L., Cloke, H. L., Neal, J. C., Freer, J., & Bates, P. D. (2015). Satellite-supported flood forecast in river networks: A real case study. *Journal of Hydrology*. http://dx.doi.org/10.1016/j.hydrol.2015.01.084.

Garcia-Pintado, J., Neal, J. C., Mason, D. C., Dance, S., & Bates, P. (2013). Scheduling satellite-based SAR acquisition for sequential assimilation of water level observations into flood modelling. *Journal of Hydrology*, 495, 252–266.

Gruber, A., Wessel, B., Huber, M., Breunig, M., Wagenbreener, S., & Roth, A. (2012). Quality assessment of first TanDEM-X DEMs for different terrain types. *9th European Conference on Synthetic Aperture Radar Program*.

Horritt, M. S., Mason, D. C., Cobby, D. M., Davenport, I. J., & Bates, P. D. (2003). Waterline mapping in flooded vegetation from airborne SAR imagery. *Remote Sensing of Environment*, 85, 271–281.

JPL (2015a). Surface Water and Ocean Topography (SWOT) Project: Science requirements document. Available online: https://swot.jpl.nasa.gov/files/swot/SRD_021215.pdf.

JPL (2015b). SWOT: The surface water and ocean topography mission. (Eds. Fu, L-L., Alsdorf, D., Morrow, R. & Rodriguez, E.). Available online: https://swot.jpl.nasa.gov/files/swot/SWOT_MSD_1202012.pdf.

Kervrann, C. (2004). A adaptive window approach for image smoothing and structures preserving. *Proc. Eur. Conf. Computer Vision (ECCV'04), Prague, Czech Republic, May 2004.*

Krieger, G., Moreira, A., Fielder, H., Hajnsek, I., Zink, M., & Eineder, M. (2006). TanDEM-X: Mission concept, product definition and performance prediction. *Proc. European Conference on Synthetic Aperture Radar (EUSAR), Dresden, 16–18 May 2006.*

LeFavour, G. (2005). Water slope and discharge in the Amazon River estimated using the shuttle radar topography mission digital elevation model. *Geophysical Research Letters*, 32(17). http://dx.doi.org/10.1029/2005gl023836.

Martinis, S., Twele, A., & Voigt, S. (2011). Unsupervised extraction of flood-induced backscatter changes in SAR data using Markov image modeling on irregular graphs. *IEEE Transactions on Geoscience and Remote Sensing*, 49(1), 251–263.

Mason, D. C., Garcia-Pintado, J., & Dance, S. L. (2014). Improving flood inundation monitoring and modelling using remotely sensed data. *Civil Engineering Surveyor, February, 2014* (pp. 34–37).

Mason, D. C., Davenport, I. J., Neal, J. C., Schumann, G. J. -P., & Bates, P. D. (2012a). Near real-time flood detection in urban and rural areas using high resolution Synthetic Aperture Radar images. *IEEE Transactions on Geoscience and Remote Sensing*, 50(8), 3041–3052.

Mason, D. C., Schumann, G. J. -P., Neal, J. C., Garcia-Pintado, J., & Bates, P. D. (2012b). Automatic near real-time selection of flood water levels from high resolution Synthetic Aperture Radar images for assimilation into hydraulic models: A case study. *Remote Sensing of Environment*, 124, 705–716.

Mason, D. C., Scott, T. R., & Wang, H. -J. (2006). Extraction of tidal channel networks from airborne LiDAR data. *ISPRS Journal of Photogrammetry and Remote Sensing*, 61, 67–83.

Mason, D. C., Amin, M., Davenport, I. J., Flather, R. A., Robinson, G. J., & Smith, J. A. (1999). Measurement of recent intertidal sediment transport in Morecambe Bay using the waterline method. *Estuarine, Coastal and Shelf Science*, 49, 427–456.

Matgen, P., Hostache, R., Schumann, G., Pfister, L., Hoffmann, L., & Savenije, H. H. G. (2011). Towards an automated SAR-based flood monitoring system: lessons learned from two case studies. *Physics and Chemistry of the Earth*, 36, 241–252.

Morton, D., Rowland, C., Meek, L., Marston, C., Smith, G., Wadsworth, R., & Simpson, I. C. (2011). Final report for LCM2007 — The new UK land cover map. *CS technical report no 11/07.* Centre for Ecology & Hydrology, Natural Environment Research Council.

Neal, J., Schumann, G., & Bates, P. (2012). A subgrid channel model for simulating river hydraulics and floodplain inundation over large and data sparse areas. *Water Resources Research*, 48(11), W11506. http://dx.doi.org/10.1029/2012wr012514.

Neal, J. C., Schumann, G. J. -P., Fewtrell, T., Budimir, M., Bates, P. D., & Mason, D. C. (2011). Evaluating a new LISFLOOD-FP formulation with data from the summer 2007 floods in Tewkesbury, UK. *Journal of Flood Risk Management*, 4(2), 88–95 (ISSN 1753-318X).

Pappenberger, F., Dutra, E., Wetterhall, F., & Cloke, H. L. (2012). Deriving global flood hazard maps of fluvial floods through a physical model cascade. *Hydrology and Earth System Sciences*, 16, 4143–4156. http://dx.doi.org/10.5194/hess-16-4143-2012.

Patro, S., Chatterjee, C., Singh, R., & Raghuwanshi, N. S. (2009). Hydrodynamic modelling of a large flood-prone river system in India with limited data. *Hydrological Processes*, 23(19), 2774–2791. http://dx.doi.org/10.1002/hyp.7375.

Raclot, D. (2006). Remote sensing of water levels on floodplains: a spatial approach guided by hydraulic functioning. *International Journal of Remote Sensing*, 27, 2553–2574.

Rodríguez, E., Morris, C. S., & Belz, J. E. (2006). A global assessment of the SRTM performance. *Photogrammetric Engineering and Remote Sensing*, 72(3), 249–260.

Sanders, B. F. (2007). Evaluation of on-line DEMs for flood inundation modeling. *Advances in Water Resources*, 30(8), 1831–1843. http://dx.doi.org/10.1016/j.advwatres.2007.02.005.

Schumann, G., Matgen, P., Cutler, M. E. J., Black, A., Hoffmann, L., & Pfister, L. (2008). Comparison of remotely sensed water stages from LiDAR, topographic contours and SRTM. *ISPRS Journal of Photogrammetry and Remote Sensing, 63*(3), 283–296. http://dx.doi.org/10.1016/j.isprsjprs.2007.09.004.

Schumann, G. J-P., Neal, J. C., Mason, D. C., & Bates, P. D. (2011). The accuracy of sequential aerial photography and SAR data for observing urban flood dynamics, a case study of the UK summer 2007 floods. *Remote Sensing of Environment, 115*, 2536–2546.

Thornhill, G. D., Mason, D. C., Dance, S. L., Lawless, A. S., & Nichols, N. K. (2012). Integration of 3D variational data assimilation with a coastal area morphodynamic model. *Coastal Engineering, 69*, 82–96. http://dx.doi.org/10.1016/j.coastaleng.2012.05.010.

Wang, W., Yang, X., & Yao, T. (2012). Evaluation of ASTER GDEM and SRTM and their suitability in hydraulic modelling of a glacial lake outburst flood in southeast Tibet. *Hydrological Processes, 26*(2), 213–225. http://dx.doi.org/10.1002/hyp.8127.

Yamazaki, D., O'Loughlin, F., Trigg, M. A., Miller, Z. F., Pavelsky, T. M., & Bates, P. D. (2014). Development of the globalwidth database for large rivers. *Water Resources Research, 50*, 3467–3480. http://dx.doi.org/10.1002/2013WR014664.

Yan, K., Di Baldassarre, G., Solomatine, D. P., & Schumann, G. J. -P. (2015). A review of low-cost space-borne data for flood modelling: topography, flood extent and water level. *Hydrological Processes*. http://dx.doi.org/10.1002/hyp.10449.

Yan, K., Di Baldassarre, G., & Solomatine, D. P. (2013). Exploring the potential of SRTM topographic data for flood inundation modelling under uncertainty. *Journal of Hydroinformatics, 15*(3), 849. http://dx.doi.org/10.2166/hydro.2013.137.

Zink, M. (2012). TanDEM-X mission status. *Proc. IGARSS Symp., Munich, Germany, July 22–27, 2012*.